

Leading-order seismic imaging using curvelets

Huib Douma*, formerly Colorado School of Mines, now at Princeton University, Princeton, NJ 08544, USA
Maarten V. de Hoop, Purdue University, West Lafayette, IN 47907, USA

Summary

Using common-offset migration in a constant background medium as an example, we show that using curvelets as building blocks of seismic data, the Kirchhoff diffraction-stack can, to leading-order in angular frequency, horizontal wavenumber, and migrated location, be rewritten as a transformation of coordinates of the curvelets in the data, combined with amplitude scaling. This transformation is calculated using map migration which uses the local slopes provided by the curvelet decomposition of the data. This transformation includes the earlier proposed method of imaging with curvelets consisting of a translation, rotation and dilation, but in addition incorporates a shear deformation of each curvelet and a dilation term that (to leading order) corrects for both the focussing or defocussing of curvelets upon imaging and geometrical spreading. The accuracy of the method is verified using a numerical example that indicates that using the leading-order approximation only, provides a good approximation to migration in a constant background medium. The essence of the presented leading-order derivation applies to heterogeneous media also.

Introduction

Recently curvelets have been shown to optimally sparsify smooth functions away from singularities along smooth curves (Candès & Donoho, 2004). Since the wavefronts in seismic data lie mainly along smooth surfaces (or curves in two dimensions) and since the imaging operator belongs to the class of operators that is sparsified by curvelets (Smith, 1998; Candès & Demanet, 2005), curvelets are plausible candidates for simultaneous sparse representation of both the seismic data and the imaging operator. In a nutshell, a curvelet can be viewed as a piece of a bandlimited plane wave that is in the Fourier domain localized near a wedge (see Figure 1a) indexed by a scale index j and an angular index l (determining its frequency content and its main associated direction, respectively). The tiling of the Fourier domain is particular in that the length of each wedge is proportional to its squared width (*parabolic scaling*). Each curvelet can be moved in the spatial domain over a grid associated with each wedge (Figure 1b). The location on this spatial grid is indexed by two translation indices m_1 and m_2 . Therefore, a curvelet is uniquely identified by multi-index $\mu = (j, l, m_1, m_2)$. Because curvelets constitute a tight frame (which can be thought of as a non-orthogonal basis) for L^2 , they satisfy $\forall f \in L^2(\mathbb{R}^2)$ the reconstruction formula

$$f = \sum_{\mu \in \mathcal{M}} (f, c_\mu) c_\mu, \quad (f, c_\mu) = \int_{\mathbb{R}^2} f(x) c_\mu^*(x) dx. \quad (1)$$

From the Kirchhoff diffraction-stack to a coordinate transformation of curvelets

In the following derivation we use migration in a constant background medium as an example but emphasize that the essence of the derivation continues to hold for migration in heterogeneous media. The common-offset (CO) 2.5-D time-migration equation is given by (Bleistein *et al.*, 2000,

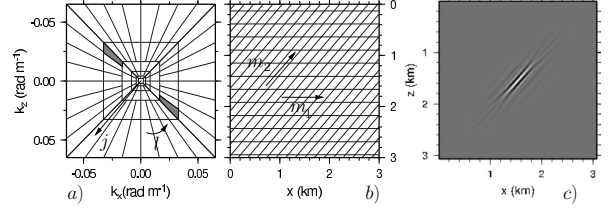


Fig. 1: (a) Digital curvelet tiling of Fourier domain into wedges, (b) spatial tiling associated with grey wedge shown in a, and (c) a curvelet in the spatial domain.

p.309, equation (6.3.25))

$$\beta(\mathbf{y}) = \int_{-\infty}^{\infty} \int_{-\infty}^{\infty} \sqrt{|\omega|} a(\mathbf{y}, x; h) e^{-i\omega(r_s+r_g)/v+i(\pi/4)\text{sgn}\omega} \times U_s(x, \omega) dx d\omega, \quad (2)$$

where $\beta(\mathbf{y})$ is the reflectivity function at migrated location $\mathbf{y} = (y_1 y_2)^T$, ω is the angular frequency, and $U_s(x, \omega)$ denotes the scattered field at midpoint location x , Fourier transformed with respect to time t , and h is the half-offset. Figure 2 shows the geometry associated with 2-D CO time-migration. The amplitude $a(\mathbf{y}, x; h)$ is given by

$$a(\mathbf{y}, x; h) = \frac{4y_2}{\sqrt{2\pi v^3}} \frac{\sqrt{r_s+r_g} (r_s^2+r_g^2)}{(r_s r_g)^{3/2}} \cos\theta(x, \mathbf{y}; h), \quad (3)$$

with $\theta(x, \mathbf{y}; h)$ half the opening angle between the slowness vectors at the source and the receiver locations, v the medium velocity, and r_s and r_g the distances from the source and the receiver to the reflector location, respectively, given by $r_{s,g} = r_{s,g}(\mathbf{y}, x; h) = \sqrt{(x \pm h - y_1)^2 + y_2^2}$, where the minus-sign in the r.h.s. relates to the source location (r_s) and the plus-sign to the receiver location (r_g). Anticipating that in the spectral domain a curvelet is localized near a wedge, we Fourier transform U_s with respect to x [using the convention given in Bleistein *et al.* (2000, p.29-30)] to get

$$\beta(\mathbf{y}) = \frac{1}{2\pi} \int_{-\infty}^{\infty} \int_{-\infty}^{\infty} \sqrt{|\omega|} \hat{U}_s(k_x, \omega) e^{i(\pi/4)\text{sgn}\omega} \times \left[\int_{-\infty}^{\infty} a(\mathbf{y}, x; h) e^{-i\{\omega(r_s+r_g)/v-k_x x\}} dx \right] dk_x d\omega. \quad (4)$$

The quantity between the square brackets is an oscillatory integral that can be approximated using the method of stationary phase [e.g., Bleistein *et al.* (2000, p.129)]. Treating $-\omega$ as the formal large parameter and defining the phase Φ as

$$\Phi(\mathbf{y}, x, k_x, \omega; h) := \frac{r_s(\mathbf{y}, x; h) + r_g(\mathbf{y}, x; h)}{v} - \frac{k_x}{\omega} x, \quad (5)$$

we get

$$\beta(\mathbf{y}) = \int_{-\infty}^{\infty} \int_{-\infty}^{\infty} \frac{a(\mathbf{y}, x(\mathbf{y}, k_x/\omega; h); h)}{\sqrt{2\pi} |\Phi''(\mathbf{y}, x(\mathbf{y}, k_x/\omega; h), k_x, \omega; h)|} \times e^{-i\omega\Phi(\mathbf{y}, x(\mathbf{y}, k_x/\omega; h), k_x, \omega; h)} \hat{U}_s(k_x, \omega) dk_x d\omega, \quad (6)$$

Leading-order seismic imaging using curvelets

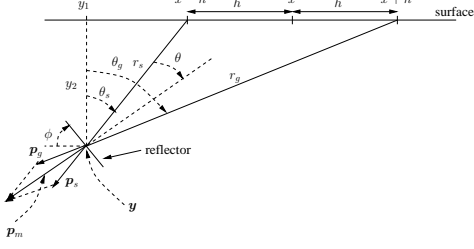


Fig. 2: Geometry associated with 2-D CO time migration.

with $\Phi''(\mathbf{y}, x(\mathbf{y}, k_x/\omega; h), k_x, \omega; h) := \partial^2 \Phi / \partial x^2|_{x(\mathbf{y}, k_x/\omega; h)}$ the Hessian evaluated at the stationary midpoint location $x(\mathbf{y}, k_x/\omega; h)$ and where we used that the Hessian turns out to be positive definite.

Let $\beta_\mu(\mathbf{y})$ be the image of one input curvelet c_μ , with multi-index $\mu = (j, l, m_1, m_2)$. That is, we replace the input data $\tilde{U}_s(k_x, \omega)$ in equation (6) with one curvelet $\hat{c}_\mu(k_x, \omega)$, where the notation \hat{c}_μ denotes the Fourier transform of the curvelet $c_\mu(x, t)$ in the $x - t$ domain. Therefore we have

$$\beta_\mu(\mathbf{y}) = \int_{-\infty}^{\infty} \int_{-\infty}^{\infty} a'(\mathbf{y}, k_x, \omega; h) e^{-iP(\mathbf{y}, x(\mathbf{y}, k_x/\omega; h), k_x, \omega; h)} \times \hat{c}_\mu(k_x, \omega) dk_x d\omega, \quad (7)$$

where we have defined

$$a'(\mathbf{y}, k_x, \omega; h) := \frac{a(\mathbf{y}, x(\mathbf{y}, k_x/\omega; h); h)}{\sqrt{2\pi |\Phi''(\mathbf{y}, x(\mathbf{y}, k_x/\omega; h), k_x, \omega; h)|}}, \quad (8)$$

and

$$P(\mathbf{y}, k_x, \omega; h) := \omega \Phi(\mathbf{y}, x(\mathbf{y}, k_x/\omega; h), k_x, \omega; h) = \omega t(\mathbf{y}, x(\mathbf{y}, k_x/\omega; h); h) - k_x x(\mathbf{y}, k_x/\omega; h), \quad (9)$$

with

$$t(\mathbf{y}, x(\mathbf{y}, k_x/\omega; h); h) := (r_s(\mathbf{y}, x; h) + r_g(\mathbf{y}, x; h))/v \quad (10)$$

the traveltime from the source to the reflector and back to the receiver. Equation (7) is reminiscent of plane-wave migration (Akbar *et al.*, 1996).

Noticing that $\hat{c}_\mu(k_x, \omega)$ is localized near a wedge with center angular frequency ω_u and center horizontal wavenumber k_x^u , we linearize the dependence of P on ω and k_x around ω_u and k_x^u . This means that, apart from the amplitude a' , the oscillatory integral on the right-hand side of equation (7) becomes simply an inverse Fourier transform. Doing this, we have

$$P(\mathbf{y}, k_x, \omega; h) \approx P(\mathbf{y}, k_x^u, \omega_u; h) + (\omega - \omega_u) \left. \frac{dP}{d\omega} \right|_{(k_x^u, \omega_u)} + (k_x - k_x^u) \left. \frac{dP}{dk_x} \right|_{(k_x^u, \omega_u)}, \quad (11)$$

where the derivatives $dP/d\omega$ and dP/dk_x denote total derivatives. From equation (9) it is immediate that

$$P(\mathbf{y}, k_x^u, \omega_u; h) = \omega_u t(\mathbf{y}, x(\mathbf{y}, p_u; h); h) - k_x^u x(\mathbf{y}, p_u; h), \quad (12)$$

where $p_u := k_x^u/\omega_u$. Then, calculating the total derivative, it follows from equation (9) that

$$\left. \frac{dP}{d\omega} \right|_{(k_x^u, \omega_u)} = t(\mathbf{y}, x(\mathbf{y}, p_u; h); h) + \left(\omega \frac{\partial t}{\partial \omega} \frac{\partial x}{\partial \omega} \right) \Big|_{(k_x^u, \omega_u)} - \left(k_x \frac{\partial x}{\partial \omega} \right) \Big|_{(k_x^u, \omega_u)}. \quad (13)$$

Since $p = \partial t / \partial x$ and $\omega p = k_x$, it follows that

$$\left. \frac{dP}{d\omega} \right|_{(k_x^u, \omega_u)} = t(\mathbf{y}, x(\mathbf{y}, p_u; h); h). \quad (14)$$

Similarly, it follows that

$$\left. \frac{dP}{dk_x} \right|_{(k_x^u, \omega_u)} = -x(\mathbf{y}, p_u; h). \quad (15)$$

Using equations (12), (14), and (15) in (11), we have

$$P(\mathbf{y}, k_x, \omega; h) \approx \omega t(\mathbf{y}, x(\mathbf{y}, p_u; h); h) - k_x x(\mathbf{y}, p_u; h). \quad (16)$$

In addition, using that the amplitude $a'(\mathbf{y}, k_x, \omega; h)$ varies slowly over the spectral support (i.e., a spectral wedge) of a curvelet, we approximate $a'(\mathbf{y}, k_x, \omega; h) \approx a'(\mathbf{y}, k_x^u, \omega_u; h)$. Then, using this together with equation (16) in (7), it follows that

$$\beta_\mu(\mathbf{y}) = a'(\mathbf{y}, k_x^u, \omega_u; h) \int_{-\infty}^{\infty} \int_{-\infty}^{\infty} \hat{c}_\mu(k_x, \omega) \times e^{-i\{\omega t(\mathbf{y}, x(\mathbf{y}, p_u; h); h) - k_x x(\mathbf{y}, p_u; h)\}} dk_x d\omega, \quad (17)$$

which is indeed an inverse Fourier transform of a curvelet.

Furthermore, we make use of the fact that curvelets remain (fairly) localized in the spatial domain under the action of the migration operator. That is, given a curvelet in the data $c_\mu(x, t)$ with center location (x_u, t_u) and dominant slope p_u , this curvelet is localized near the map-migrated location $\mathbf{y}_m = \mathbf{y}_m(x_u, t_u, p_u)$. Therefore, we linearize $t(\mathbf{y}, x(\mathbf{y}, p_u; h); h)$ and $x(\mathbf{y}, p_u; h)$ in \mathbf{y} around the map-migrated location \mathbf{y}_m . Linearizing $x(\mathbf{y}, p_u; h)$ gives

$$x(\mathbf{y}, p_u; h) \approx x_u + (\nabla_{\mathbf{y}} x(\mathbf{y}, p_u; h))|_{\mathbf{y}_m} \cdot (\mathbf{y} - \mathbf{y}_m), \quad (18)$$

where we used $x_u = x(\mathbf{y}_m, p_u; h)$ and where the notation $\nabla_{\mathbf{y}}$ denotes the gradient with respect to \mathbf{y} . Linearizing $t(\mathbf{y}, x(\mathbf{y}, p_u; h); h)$ in \mathbf{y} again involves total derivatives instead of partial derivatives since both t and x depend on \mathbf{y} . Hence, we have

$$t(\mathbf{y}, x(\mathbf{y}, p_u; h); h) \approx t(\mathbf{y}_m, x(\mathbf{y}_m, p_u; h); h) + \left. \frac{dt(\mathbf{y}, x(\mathbf{y}, p_u; h); h)}{d\mathbf{y}} \right|_{\mathbf{y}_m} \cdot (\mathbf{y} - \mathbf{y}_m) = t_u + (\mathbf{y} - \mathbf{y}_m) \cdot \left\{ \nabla_{\mathbf{y}} t(\mathbf{y}, x(\mathbf{y}, p_u; h); h)|_{\mathbf{y}_m} + p_u \nabla_{\mathbf{y}} x(\mathbf{y}, p_u; h)|_{\mathbf{y}_m} \right\} \quad (19)$$

Using equations (18) and (19) in (17), while realizing that the integral is peaked at $\mathbf{y} = \mathbf{y}_m$ (i.e., we can replace $a'(\mathbf{y}, k_x^u, \omega_u; h)$ in equation (17) with $a'(\mathbf{y}_m, k_x^u, \omega_u; h)$) and at the same time recognizing the inverse Fourier transform, we finally have

$$\beta_\mu(\mathbf{y}) = a'(\mathbf{y}_m, k_x^u, \omega_u; h) c_\mu(L \cdot (\mathbf{y} - \mathbf{y}_m) + \mathbf{x}_u), \quad (20)$$

where we have defined

$$L := \left(\left\{ \nabla_{\mathbf{y}} t(\mathbf{y}, x(\mathbf{y}, p_u; h); h) + p_u \nabla_{\mathbf{y}} x(\mathbf{y}, p_u; h) \right\} |_{\mathbf{y}_m}, \nabla_{\mathbf{y}} x(\mathbf{y}, p_u; h) |_{\mathbf{y}_m} \right) \quad (21)$$

and $\mathbf{x}_u := (x_u \ t_u)^T$. Therefore, it follows that *to leading-order in angular frequency, horizontal wavenumber, and migrated location, Kirchhoff diffraction becomes a coordinate transformation of the curvelets in the data*, given by

$$\mathbf{y} = L^{-1} \cdot (\mathbf{x} - \mathbf{x}_u) + \mathbf{y}_m, \quad (22)$$

Leading-order seismic imaging using curvelets

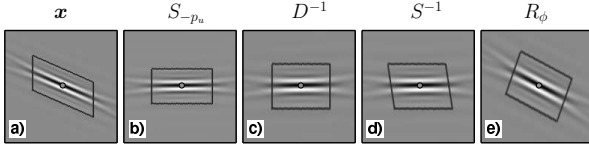


Fig. 3: Illustration of the individual components of the linear transformation $R_{\phi} \cdot S^{-1} \cdot D^{-1} \cdot S_{-p_u}$: input curvelet (a) after S_{-p_u} (b), D^{-1} (c), S^{-1} (d), and R_{ϕ} (e).

combined with an amplitude scaling, where both the matrix L and the amplitude a' are evaluated with the use of (2D) pre-stack map migration (Douma & de Hoop, 2006, their equations (7), (8), and (11) restricted to 2D). Hence, using curvelets as building blocks of seismic data, the integration along diffraction surfaces is replaced with a simple coordinate transformation of each curvelet.

Now that we know the leading-order approximation to one CO time-migrated curvelet c_{μ} through equation (20), we can determine the total image of the (scattered) data u_s using the reconstruction formula (1). Letting M denote the 2.5-D CO time-migration operator and assuming that seismic data can be sparsely represented with curvelets, we have

$$\beta(\mathbf{y}) = \sum_{\mu \in \mathcal{M}} (u_s, c_{\mu}) [M c_{\mu}](\mathbf{y}) = \sum_{\mu \in \mathcal{M}} (u_s, c_{\mu}) \beta_{\mu}(\mathbf{y}), \quad (23)$$

with $\beta_{\mu}(\mathbf{y})$ given by equation (20), and \mathcal{M} the index set that holds the multi-indices of curvelets that survive a certain threshold. Note that the index set \mathcal{M} is determined through thresholding the projection of the seismic data u_s onto the curvelet frame.

For constant background media and a CO acquisition geometry the matrix L can be written as a sequence of matrix multiplications given by

$$\mathbf{y} = R_{\phi} \cdot S^{-1} \cdot D^{-1} \cdot S_{-p_u} \cdot (\mathbf{x} - \mathbf{x}_u) + \mathbf{y}_m, \quad (24)$$

where R_{ϕ} denotes a (clockwise) rotation with angle ϕ , S_{-p_u} and S are shear matrices given by

$$S_{-p_u} := \begin{pmatrix} 1 & 0 \\ -p_u & 1 \end{pmatrix}, \quad S := \begin{pmatrix} 1 & \frac{X \cos \phi - \sin \phi}{\cos \phi + X \sin \phi} \\ 0 & 1 \end{pmatrix}, \quad (25)$$

with $X := (\tan \theta_s r_s^3 + \tan \theta_g r_g^3) / (r_s^3 + r_g^3)$, and D is a dilation matrix given by

$$D := \begin{pmatrix} \cos \phi + X \sin \phi & 0 \\ 0 & 2 \cos \theta / v \end{pmatrix}. \quad (26)$$

In equations (25) and (26) θ is the half opening-angle (see Figure 2) and $\phi := (\theta_s + \theta_g) / 2$ is the migrated dip. Both θ and ϕ can be calculated using map migration. From equation (24) it follows that the leading-order approximation to CO time-migration can be described by the following sequence of transformations. First, a curvelet in the data with center location \mathbf{x}_u (i.e., center midpoint location x_u and center two-way traveltime t_u) and center slope p_u , is sheared along the time-axis to have zero slope. Subsequently, each curvelet is dilated in both the vertical and horizontal direction. The dilation in the vertical direction takes care of the stretch due to the imaging condition (Douma & de Hoop, 2005), while the dilation in the horizontal direction takes (to leading-order) care of both focussing or defocussing of curvelets upon imaging and geometrical spreading. Subsequently, each curvelet is sheared

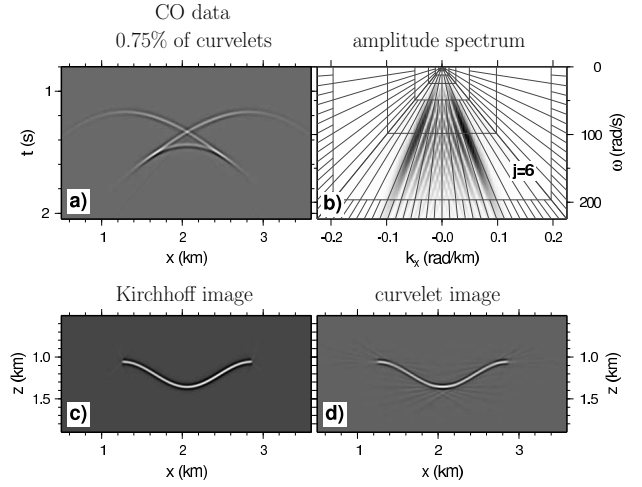


Fig. 4: Sparse representation of CO ($h = 1000$ m) data from a syncline model (a) and its associated amplitude spectrum (b). Each curvelet used to reconstruct the data shown in a is migrated using equation (20), resulting in the image in d.

along the horizontal direction and is rotated to have output dip ϕ . All these linear transformations have the center location \mathbf{x}_u of the curvelet as their origin. Finally, the resulting transformed curvelet is translated to the migrated output location \mathbf{y}_m . This sequence of transformations (except the translation) is depicted for one curvelet in Figure 3, where a parallelogram is added to allow easy identification of the geometric character of each individual matrix multiplication. Note that the coordinate transformation incorporates the rotation, dilation and translation from Douma and de Hoop (2005), but that this leading order approximation in addition incorporates a shear deformation and a dilation term that corrects to leading-order for both focussing (or defocussing) of curvelets upon imaging combined with geometrical spreading.

Numerical examples

Figure 4a shows a CO section (with offset equal 1 km) of synthetic data generated from a syncline model in a constant-velocity background. We use these data to highlight that triplications in the data are dealt with naturally; crossing events in the data are simply constructed from curvelets that have the same location but different orientations. In Figure 4a we used only the 0.75% largest curvelet coefficients of the data to reconstruct the data. This thresholding percentage was determined without the use of a sophisticated thresholding procedure but rather by visually verifying that the difference between the original and reconstructed data is negligible. The associated amplitude spectrum of the reconstructed data is shown in Figure 4b. Observe that almost all energy is contained in frequency bands associated with scale indices $4 \leq j \leq 6$. Figure 4c shows the 2.5-D CO Kirchhoff migrated result, while Figure 4d shows the curvelet-based migration calculated with the leading-order approximation [i.e., using equation (23)]. The leading-order curvelet-based migration provides a good approximation to the Kirchhoff result, with some small artefacts related to nonlinear deformation beyond the leading-order approach.

The bandlimited nature of curvelets allows the possibility to do migration velocity analysis as a function of frequency. Such analysis has physical relevance since a wave averages the medium properties upon propagation over the first Fresnel zone, which is proportional to $\sqrt{\lambda}$ (with λ the

Leading-order seismic imaging using curvelets

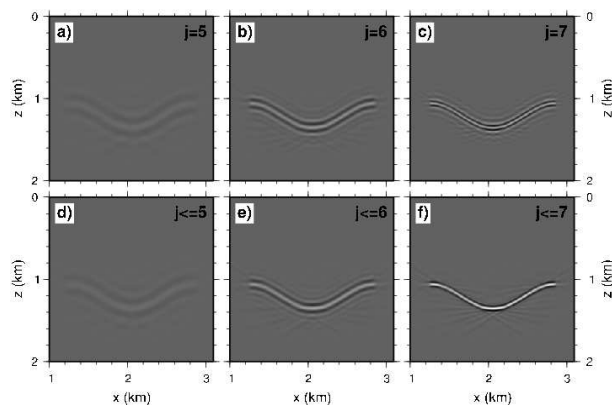


Fig. 5: Images obtained using equation (20) from the thresholded CO data shown in Figure 4a, for scales $j = 5$ (a), $j = 6$ (b), $j = 7$ (c), and for the cumulative scales $j \leq 5$ (d), $j \leq 6$ (e), and $j \leq 7$ (f).

wavelength) and thus to $1/\sqrt{\omega}$. Hence, waves of different frequencies indeed are sensitive to the earth's structure at different scales. Using curvelets in seismic imaging allows naturally for such analysis by simply choosing to image curvelets with selected frequency content (i.e., scale index) only. Although for constant background media the medium is the same at every scale, Figure 5 illustrates the principle by showing the resulting images as a function of scale-index j (Figures 5a, b and c). Figures 5d, e, and f, show the associated cumulative images. Following such per-scale imaging, the associated image gathers can then be submitted to a per-scale velocity analysis. Note that per-scale imaging in principle also allows the study of the frequency-dependence of the reflectivity. Moreover, the locally-associated directions of curvelets allow controlled illumination (Rietveld & Berkhout, 1992) of the subsurface. Figure 6a shows the amplitude spectrum of the data in Figure 4a, but reconstructed with rightward sloping curvelets only. Figure 6b shows the resulting image, which now shows the left part of the syncline only. Here, the controlled illumination is achieved by dip-filtering the *data* with curvelets. Dip-filtering the *image* with curvelets, in contrast, leads naturally to the focussing-in-dip procedure of Brandsberg-Dahl *et al.* (2003). These opportunities for frequency-dependent migration velocity-analysis and controlled illumination studies are a straightforward consequence of curvelets being appropriate building blocks of both seismic data and the imaging operator; no additional preprocessing, such as slant-stacking, is needed.

Conclusions

Using common-offset migration in a constant background medium as an example, we show that with curvelets as building blocks of seismic data Kirchhoff diffraction-stacking becomes to leading order in angular frequency, horizontal wavenumber, and migrated location, a transformation of coordinates of the curvelets in the data, combined with amplitude scaling. This transformation includes the earlier proposed method of imaging with curvelets consisting of a translation, rotation and dilation, but in addition incorporates a shear deformation of each curvelet and a dilation term that (to leading order) corrects for both focussing (or defocussing) of curvelets upon imaging and geometrical spreading. The transformation is calculated using map migration which uses the local slopes provided by the curvelet decomposition of the data. The accuracy of the method is verified using a numerical example that indicates that using the leading-order approxima-

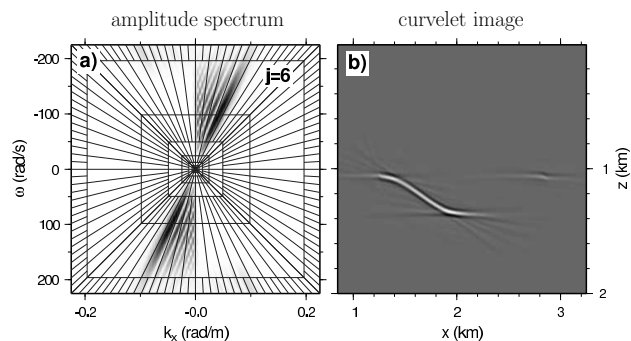


Fig. 6: Amplitude spectrum of the data in Figure 4a, but now using only rightward-sloping curvelets (a), and the resulting image of these curvelets using equation (23) (b).

tion only, provides a good approximation to migration in a constant background medium. We emphasize that the essence of the presented leading-order derivation, i.e. a stationary-phase evaluation of the integral with respect to the non-common variable combined with linearization in angular frequency, horizontal wavenumber, and migrated location, applies to heterogeneous media also.

Acknowledgments

H.D. would like to thank Roel Snieder for several useful discussions. This work was supported by the sponsors of the Consortium Project on Seismic Inverse Methods for Complex Structures at the Center for Wave Phenomena.

References

- Akbar, F., Sen, M., and Stoffa, P., 1996, Prestack plane-wave kirchhoff migration in laterally varying media: *Geoph.*, **61**, 1068–1079.
- Bleistein, N., Cohen, J., and Stockwell, J., 2000, *Mathematics of multidimensional seismic imaging, migration, and inversion*, Springer.
- Brandsberg-Dahl, S., de Hoop, M., and Ursin, B., 2003, Focusing in dip and ava compensation on scattering-angle/azimuth common image gathers: *Geoph.*, **68**, 232.
- Candès, E. J., and Demanet, L., 2005, The curvelet representation of wave propagators is optimally sparse: *Comm. on Pure and Appl. Math.*, **58**, 1472–1528.
- Candès, E. J., and Donoho, D. L., 2004, New tight frames of curvelets and optimal representations of objects with piecewise C^2 singularities: *Comm. on Pure and Appl. Math.*, **57**, 219–266.
- Douma, H., and de Hoop, M., 2005, On common-offset pre-stack time-migration with curvelets: Expanded Abstracts 75th annual international meeting of the SEG.
- Douma, H., and de Hoop, M. V., 2006, Explicit expressions for pre-stack migration in isotropic and VTI media and the applicability of map depth-migration in heterogeneous anisotropic media: *Geoph.*, **71**, S13–S28.
- Rietveld, W., and Berkhout, A., 1992, Depth migration combined with controlled illumination: *SEG Technical Program Expanded Abstracts*, **11**, 931–934.
- Smith, H., 1998, A parametrix construction for wave equations with $C^{1,1}$ coefficients: *Ann. Inst. Fourier*, **48**, 797.